Journal of Environmental Health Science and Engineering (2018) 16:213–228
https://doi.org/10.1007/s40201-018-0309-3

RESEARCH ARTICLE

Degradation of UV-filter Benzophenon-3 in aqueous solution using TiO_2 coated on quartz tubes

Nazanin Moradi [1,2] · Mohammad Mehdi Amin [1,3] · Ali Fatehizadeh [1,3] · Zahra Ghasemi [4]

Received: 15 April 2018 / Accepted: 28 July 2018 / Published online: 15 August 2018

Abstract

Background Benzophenone-3 (BP-3), one of the emerging pollutants, is commercially synthesized as UV filter used in cosmetics and other personal care products and its occurrence in the aquatic environment has widely been reported. The goal of this study was to enhance an AOP method for degradation of UV filter Benzophenone-3 in aqueous solutions.

Method In this study, sol-gel method was applied to synthesis TiO_2 nanoparticles. Subsequently, the nanoparticles were successfully coated on quartz tubes. The synthesized catalyst was characterized using XRD, FE-SEM and EDX analysis. Then, the efficiency of photocatalytic process using TiO_2 coated quartz tubes for BP-3 degradation from synthetic and real aqueous solution was assessed.

Result The optimum contact time and solution pH for the highest BP-3 degradation in the synthetic solution were found at 15 min and 10, respectively. The maximum degradation (98%) of BP-3 by photocatalytic process was observed at 1 mg/L initial BP-3 concentration using 225 cm^2 of catalyst surface area. Among the three applied kinetic models, the experimental data were found to follow the first-order equation more closely with the rate constant of 0.2, 0.048 and 0.035 1/min for 1, 3 and 5 mg/L of initial BP-3 concentration, respectively. In order to investigate the potential of this process for real effluent, the treatment of swimming pool water and wastewater treatment plant was examined and BP-3 degradation close to 88% and 32.1 was achieved, respectively.

Conclusion Based on the obtained data, the photocatalytic process could successfully be applied for water treatment in swimming pools and other effluent containing BP-3 with low turbidity. The advantage of this study is that the synthesized catalyst can be used repeatedly needless to remove catalyst from the treated solution. In addition, AOP_s can effectively eliminate organic compounds in aqueous phase, rather than transferring pollutants into another phase. The limitation of this study is that in solution with high turbidity photocatalytic degradation can be hampered and pre- treatment is needed to reduce turbidity.

Keywords Benzophenone-3 · UV filter · Photocatalysis · Swimming pool

Introduction

Benzophenone-3 (2-Hydroxy-4-methoxybenzophenone, BP-3) is an organic compound which is used in cosmetics, sunscreens, and other personal care products as UV filter [1, 2]. BP-3, as UV filter, protects human from UV radiation of the sun and conserve products' formulation [1, 3]. This aromatic compound is also used in food-packaging, pharmaceutical, and other industries [1, 4]. BP-3 has been considered as an emerging pollutant and its endocrine disruptive effects have been proved on several studies [3–5]. Dermal and oral absorption of BP-3 in rats and mice has led to alteration in their liver and kidney [6, 7]. Estrogen- dependent diseases including endometriosis in women have also been reported [8, 9]. Human exposure of BP-3 is usually through dermal application of sunscreens and other personal care products [10].

As a result of using sunscreens in recreational activities such as swimming, BP-3 can enter to the environment directly. Moreover, due to its persistence, BP-3 cannot be removed thoroughly in the wastewater treatment plants; therefore, it penetrates into the aquatic environment indirectly from the wastewater [4, 11–13].

✉ Ali Fatehizadeh
Fatehizadeh@gmail.com; A.Fatehizadeh@hlth.mui.ac.ir

1 Department of Environmental Health Engineering, School of Health, Isfahan University of Medical Sciences, Isfahan, Iran

2 Student Research Committee, School of Health, Isfahan University of Medical Sciences, Isfahan, Iran

3 Environment Research Center, Research Institute for Primordial Prevention of Non-communicable Disease, Isfahan University of Medical Sciences, Isfahan, Iran

4 Department of Fisheries, Faculty of Marine Science and Technology, University of Hormozgan, Bandar Abbas, Iran

BP-3 concentration has been reported in water and wastewater treatment plant (WWTP) effluents at the range of 29–190 μg/L, in lakes up to 345 ng/L and in rivers up to 849 ng/L [11, 14–16]. Traditional methods of wastewater treatment such as adsorption, filtration and flocculation can only transfer the organic pollutants from one phase to another which needs further treatment [17]. In the recent years, advanced oxidation process (AOP) with a promising ability to remove organic compounds, are being developed as a proper alternative to the traditional treatment methods [9, 18–20]. AOPs rely on in-situ production of highly reactive hydroxyl radicals ($OH^{\cdot}$). These reactive species are the strongest oxidants that can be applied in water and can virtually oxidize any compound present in the water matrix, often at a diffusion controlled reaction speed. Consequently, $OH^{\cdot}$ reacts unselectively once formed and contaminants will be quickly and efficiently fragmented and converted into small inorganic molecules. Hydroxyl radicals are produced with the help of one or more primary oxidants (e.g. ozone, hydrogen peroxide, oxygen) and/or energy sources (e.g. ultraviolet light) or catalysts (e.g. titanium dioxide). AOPs can reduce the concentration of contaminants from several-hundreds ppm to less than 5 ppb and therefore significantly bring COD and TOC down. The AOP procedure is particularly useful for cleaning biologically toxic or non-degradable materials such as aromatics, pesticides [21], petroleum constituents, and volatile organic compounds in wastewater [22]. The contaminant materials are converted to a large extent into stable inorganic compounds such as water, carbon dioxide and salts, and they undergo mineralization. A goal of the wastewater purification by means of AOP procedures is the reduction of the chemical contaminants and the toxicity to such an extent that the cleaned wastewater may be reintroduced into receiving streams or, at least, into a conventional sewage treatment.

As BP-3 cannot be removed completely in the conventional treatment in WWTP, some advanced processes have been studied under laboratory conditions. AOPs including oxidation with ferrate [9], ozonation and peroxone of BP-3 [23], fungal and photodegradation of BP-3 [1], BP-3 degradation using UV/H_2O_2 [24] and BP-3 degradation using persulfate catalyzed by cobalt ferrite [25] have been studied. Heterogeneous photocatalysis using semiconductors, is one of the AOPs which has an effective ability to remove organic compounds [17]. Application of TiO_2nanoparticles, especially in anatase polymorphic form, has been reported for degradation of different organic pollutants such as dyes [18], Diethyl phthalate [19], and BP-3 [20] . Mesoporous structure of this catalyst provides a large surface area for molecular transfer and enhances the degradation process [18].

Using suspension form of TiO_2 nanoparticles in the real wastewater treatment plants can result in high operational cost, because particles have to be separated from the solution [26]. Design and operation of following units may become impossible if the nanoparticles are not removed from the solution. In addition, nanoparticles cannot be used again after separation because their recycling is time-consuming and expensive [17]. On the other hand, as TiO_2 nanoparticles are activated under light radiation, aggregation of ultrafine suspended particles at the high catalyst loads inhibits light's penetration and scattering into the solution; subsequently, the pollutant degradation process would be hampered [26].

Response surface methodology (RSM) has been applied in several studies to optimize the condition under which the most degradation efficiency of organic compounds would occur. RSM consists of a group of mathematical and statistical techniques for optimizing a response which is influenced by several independent variables [18, 20, 27, 28]. Central composite design (CCD) is the most appropriate model used for optimizing the condition under RSM design [28].

To the best of our knowledge this is the first time that TiO_2 coated on quartz tube was applied for BP-3 degradation. The method used in this study was superior to the other related studies in which TiO_2 nanoparticles was used as the catalyst [20, 26], because as apposed to those studies, in this study nanoparticles were coated on quartz tubes, so that no particles aggregation occurred. The best advantage of this method is that the catalyst can be used repeatedly and for a long time for BP-3 degradation in aqueous solution. In This study BP-3 existence in the swimming pools and wastewater treatment plant was investigated in our country (Iran) for the first time. Modeling and optimizing the photodegradation process using RSM was carried out. The results showed the ability of the applied method for treatment of real aqueous solutions containing BP-3 especially swimming pools.

Materials and methods

Chemicals

Titanium tetra-isopropoxide (TTIP) 97%, 2-Hydroxy-4-methoxy benzophenone (BP-3) 98%, N, O-Bis (trimethysilyl) trifluroacetamide (BSTFA) 99.0% were purchased from Sigma Aldrich. 2-Propanol dried 99.99%, Acetone 99.9%, methanol, CCl_4, Hydrochloric acid and Sodium hydroxide were supplied from Merck. All chemicals were analytical reagent grade. The quartz tubes with 8 mm inner diameter, 10 mm outer diameter and 8 cm height were purchased from Alvandshimi Company, Iran. The molecular structure and chemical properties of BP-3 are summarized in Table 1.

Table 1 Characteristics of BP-3

Molecular structure	Chemical formula	Molecular weight(g/mol)	CAS number
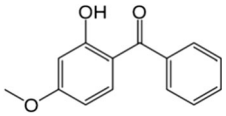	$C_{14}H_{12}O_3$	228.24	131–57-7

Synthesis of TiO_2 nanoparticles and coating on quartz tubes

Five quartz tubes were thoroughly cleaned by concentrated acetone and immersed in NaOH (1 M) for 24 h in order to hydrophilization. Then, the tubes were washed by distilled water. TiO_2 nanoparticles were synthesized via sol-gel method. First, 20 ml of HCl (0.1 M) was added to 880 ml of dried 2-propanol under vigorous stirring (first solution). Then, 14 ml of TTIP, as a precursor of TiO_2, was dissolved into 86 ml of dried 2-propanol (second solution). Afterwards, the second solution was added slowly to the first solution under stirring. The solution was agitated for 5 h at 0 °C [29].

All tubes were completely immersed in TiO_2 sol solution for 30 min and slowly taken out and dried in microwave for 10 min. To achieve uniform and strong layer of TiO_2 nanoparticles on the surface of the tubes, the mentioned procedure was repeated for 6 times. Subsequently, the tubes and remained sol solution were dried at 105 °C for 24 h and calcined at 550 °C for 2 h. Figure 1 shows the flow diagram of preparing the TiO_2 sol and the synthesized catalyst.

Characterization of the catalyst

The coated tubes and nano- powder of TiO_2 were characterized by X-ray diffraction (XRD) (Philips, PW1730) using Cu radiation in $2\theta = 0–80°$. The current and voltage were 30 mA

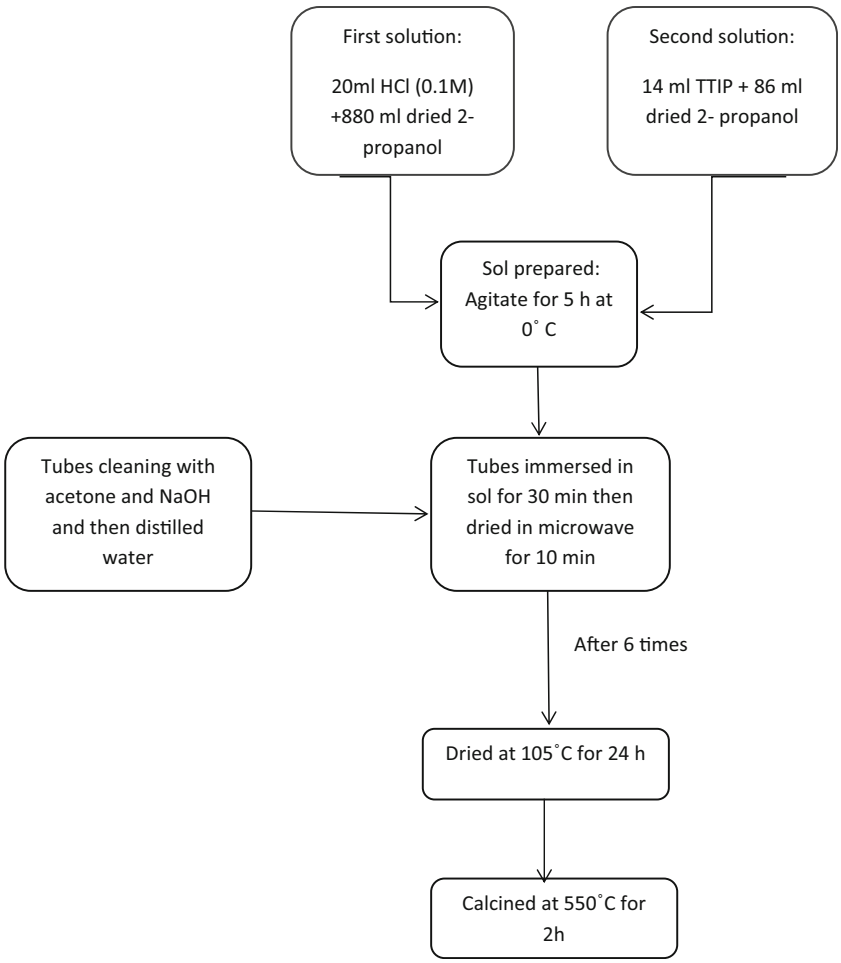

Fig. 1 Flow diagram of preparing the TiO_2 sol and the synthesized catalyst

and 40 kV, respectively. Using Debye- Scherer's equation, the average crystal size of anatase form of synthesized catalyst was calculated (Eq. 1).

$$D = \frac{k \times \lambda}{\beta \times \cos\theta} \quad (1)$$

Where D is crystal size (nm), K is dimensionless shape factor, λ is the x-ray wavelength (nm), β is the line broadening at half the maximum intensity (FWHM) and θ is the Bragg angle (degree).

Scanning electron microscope (SEM) (TE scan) was used to obtain the morphology of TiO_2 nanoparticles which were coated on quartz tubes. Energy dispersive X-ray analysis (EDX) was also applied to provide elemental identification and quantitative information of TiO_2 nano-powder and coated tubes.

Photocatalytic process set up

The experiments of the BP-3 degradation were carried out in a cubic- Plexiglas reactor with 750 ml solution capacity. An UV lamp (250 W, 360–400 nm) was mounted above the reactor (3 cm above solution). The tubes were placed in a holder into the reactor that could be easily taken out from the solution. BP-3 can hardly dissolve into water; therefore, stock solution (1 g/L) was prepared in methanol. To achieve subsequent concentrations, the stock was diluted by distilled water. The following parameters were examined and optimized: initial BP-3 concentration (1–5 mg/L), catalyst surface area (45–225 cm^2), pH (3–10), contact time (5–60 min). The experiments were conducted in triplicate experiments and average values were reported. The photocatalytic process was operated in a controlled temperature (20 ± 1 °C) by a water bath. BP-3 removal efficiency was calculated using Eq. (2).

$$R(\%) = \frac{C_0 - C_e}{C_0} \times 100 \quad (2)$$

Where C_0 is initial BP-3 concentration and C is effluent BP-3 concentration.

In order to investigate the potential of photocatalytic process for real effluent, the contaminated water was collected from a swimming pool (Isfahan, Iran). The characteristics of the swimming pool are summarized in Table 2. Also a sample of a wastewater treatment plant (Isfahan, Iran) was collected and tested by the method. The characteristics of the wastewater are shown in Table 3.

Photocatalytic process optimization by RSM

Central composite design (CCD) and RSM methodology were applied for optimization the BP-3 photo-degradation. Experiments' design was conducted by STATISTICA software (version 10). 4 parameters including solution pH, catalyst surface area, BP-3 initial concentration and contact time were introduced into the software in five levels as -α, −1, 0, 1, +α (Table 4). Eq. (3) was used to calculate the number of CCD experiments.

$$Ex_{No.} = 2^N + 2N + n \quad (3)$$

where N is the number of variables and n is central points. The terms 2^N and 2 N show factorial and axial experiments, respectively. Based on the Eq. (3), 24 experiments and 6 repetitions were constructed as shown in Table 5.

The response of CCD was predicted by Eq. (4).

$$Y = b_0 + \sum_{i=1}^{k} b_i x_i + \sum_{i=1}^{k} b_{ii} x_i^2 + \sum_{i=1}^{k=1} \sum_{j=2}^{k} b_{ij} x_i x_j + \varepsilon \quad (4)$$

where Y is the predicted response, x_i, x_j, … x_k are the input variables, x_i^2, x_j^2, … x_k^2 are the square effects, b_0 is the intercept term, b_i is the linear effect, b_{ii} is the squared effect, b_{ij} is the interaction effect and ε is the random error [30, 31].

Table 2 Properties of the swimming pool water

Parameter	value
BP-3 Conc. (mg/L)	0.07
EC (μS/cm)	1885 ± 140
pH	7.46 ± 0.28
Salinity (%)	0.08 ± 0.001
Turbidity (NTU)	2.25 ± 0.1

Analytical method

Sample preparation and dispersive liquid-liquid microextraction (DLLME) procedure

In each experiment after the reaction time, 5 mL of the solution was extracted from the reactor and solution pH was adjusted at 4, using HCl and NaOH (0.1 M). Afterwards, 500 μL of acetone containing 50 μL CCL_4 was rapidly injected into the solution. The cloudy solution was centrifuged at 5000 rpm for 5 min (Hettich, Universal 320). After phase separation, 30 μL of sediment solution was extracted and transferred into 1.5 mL gastight vial [32].

Table 3 Properties of the collected wastewater

Parameter	value
BP-3 Conc. (mg/L)	0.0056
EC (μS/cm)	1261 ± 140
pH	7.41 ± 0.28
TSS	496
Turbidity (NTU)	285 ± 10

Table 4 Ranges and levels of the input data

Variables	Range and level				
	-α	-1	0	+1	A
pH (p)	6	7	9	10	12
Time (t), min	10	15	20	25	30
Initial concentration (c), mg/L	1	2	3	4	5
Tube area (a),cm^2	45	90	135	180	225

Derivatization process and GC-MS analysis

The extracted solution was gently dried by nitrogen gas. Afterwards, 25 μL of BSTFA (derivatization reagent) was added to the vial. The vial was vigorously shaken using vortex (Heidolph) for 1 min and placed in water bath (type W350) at 75 °C for 5 min to enhance the reaction between BSTFA and BP-3. Then the vial was taken out and remained at room temperature for 5 min before analysis. Gas Chromatograph (Agilent 7890, USA) equipped with a mass detector (Agilent Tech., 5975C, USA) was used for analysis. GC-Mass's software was ChemStation under Microsoft XP windows. The details of detection by GC- Mass are shown in Table 6.

Validation of the analytical method

The analytical method validation was performed in accordance with the guidelines of the international conference on harmonization (ICH) [33]. Studied parameters include selectivity/specificity, linearity, limits of detection and quantitation, repeatability, inter mediate precision, accuracy and recovery are summarized in Table 7.

Table 5 Experiments design and comparison between observed and predicted results

No.	pH	Time (min)	Surface area (cm^2)	Concentration (mg/L)	Observed BP-3 removal (%)	Predicted BP-3 removal (%)
1	7	15	90	2	41.000	40.212
2	7	15	90	4	32.500	31.521
3	7	15	180	2	54.000	54.805
4	7	15	180	4	45.000	43.552
5	7	25	90	2	42.000	41.822
6	7	25	90	4	33.000	32.820
7	7	25	180	2	54.500	56.228
8	7	25	180	4	45.250	44.663
9	10	15	90	2	52.500	52.007
10	10	15	90	4	41.000	37.315
11	10	15	180	2	68.000	68.069
12	10	15	180	4	52.250	50.814
13	10	25	90	2	53.000	54.479
14	10	25	90	4	41.750	39.474
15	10	25	180	2	69.000	70.354
16	10	25	180	4	52.500	52.786
17	6	20	135	3	36.670	37.051
18	12	20	135	3	45.670	46.534
19	9	10	135	3	40.670	43.856
20	9	30	135	3	49.330	47.726
21	9	20	45	3	29.000	31.759
22	9	20	225	3	61.330	60.153
23	9	20	135	1	81.000	78.221
24	9	20	135	5	45.600	49.962
25	9	20	135	3	57.670	57.445
26	9	20	135	3	50.330	57.445
27	9	20	135	3	56.000	57.445
28	9	20	135	3	60.330	57.445
29	9	20	135	3	59.000	57.445
30	9	20	135	3	61.000	57.445

Table 6 Details of detection by GC- Mass

Item	Descriptions
GC column	DB-5 MS column (60 m × 0.25 mm i.d.; 0.25 μm film thickness; Agilent Technologies, Palo Alto, CA, USA)
Oven ramp	Initial temperature: 120 °C (held for 3 min) 60 °C per min to 280 °C (held for 5.5 min) Total run time: 11.17 min
Injection port	Temperature: 280 °C Spilt mode Split ratio: 10/1
Transfer line	300 °C
Carrier gas	Helium 99.9995% (2 ml/min)
Sample injection volume	2 μL
Ion source	230 °C
Detect acquisition mode	Selected ion monitoring (SIM)
Selected *m/z* for quantification	285

Result and discussion

Catalyst characterization

Figure 2a–c shows the XRD pattern of the bare quartz tubes, the synthesized TiO_2 nano-particles and coated quartz tubes. As it is illustrated in Fig. 2a no peak was observed for the bare quartz tubes. However, the sharpest peaks at $2\theta = 25.3$ in Fig. 2b, c show that anatase form of TiO_2 was completely achieved and also properly coated on the quartz tubes. The existence anatase peaks at $2\theta = 25.3$, 38.3, 48.2, 54.15, 68.9 and 75.35 confirm the presence of anatase TiO_2 on the coated quartz. Although, Rutile phase is also recognized on XRD pattern, it can be ignored because the ratio of Rutile phase to anatase phase is rare. The same results were reported in the literature [17, 29, 34].

Using Debye- Scherer's equation, the anatase TiO_2 average crystal size was 14.5 nm calculated from FWHM at $2\theta = 25.35$.

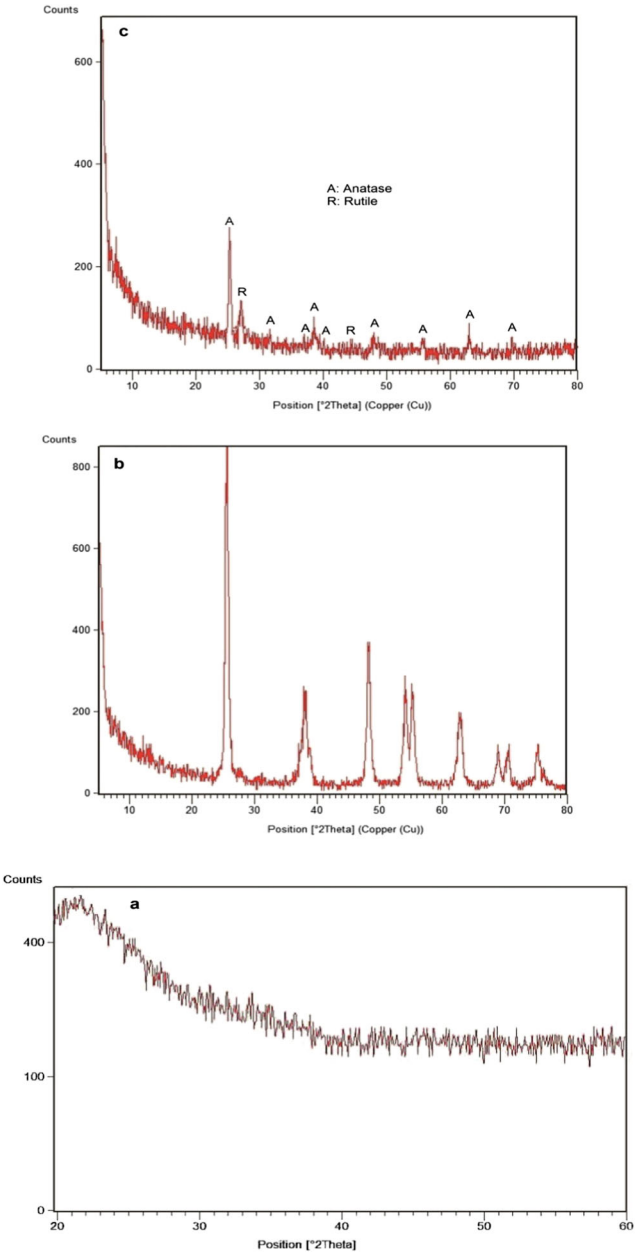

Fig. 2 XRD Pattern of bare quartz tubes (**a**), Synthesized TiO_2 (**b**) and TiO_2 coated quartz tubes (**c**)

Table 7 Main validating parameters of the method for determination of BP-3 in water

r^2	LOD[a]	LOQ[b]	LR[c]	RSD[d] (%)		Recovery (%)
				Within days	Between days	
0.998	0.007	0.023	0.1–1000	4.3	7.6	92.7

[a] limits of detection; (ppb); based on the signal to noise ratio (S/N) of 3

[b] limits of quantification; (ppb); based on the signal to noise ratio (S/N) of 10

[c] linear range; (ppb)

[d] Relative standard deviation; three replicate experiments of spiked blank plasma samples at three concentration ranges (low concentration, medium concentration and high concentration)

The morphology of synthesized TiO_2 nanocrystals in powder form and coated quartz is shown in Fig. 3a–f. Scanning electron microscope (SEM) images show uniform distribution of TiO_2 on quartz. The rough surface of coated quartz which caused by TiO_2 nanoparticles layer, provide more activated sites for photodegradation.

As it can be seen in Fig. 3b, the size given by SEM is larger than the size calculated by Scherer equation. It should note that theoretically, size obtained by XRD using Scherer equation is smaller than that by SEM [35]. The crystallite size by XRD must always be less than the particle size by SEM because the particle tested by XRD is crystallize size, or named

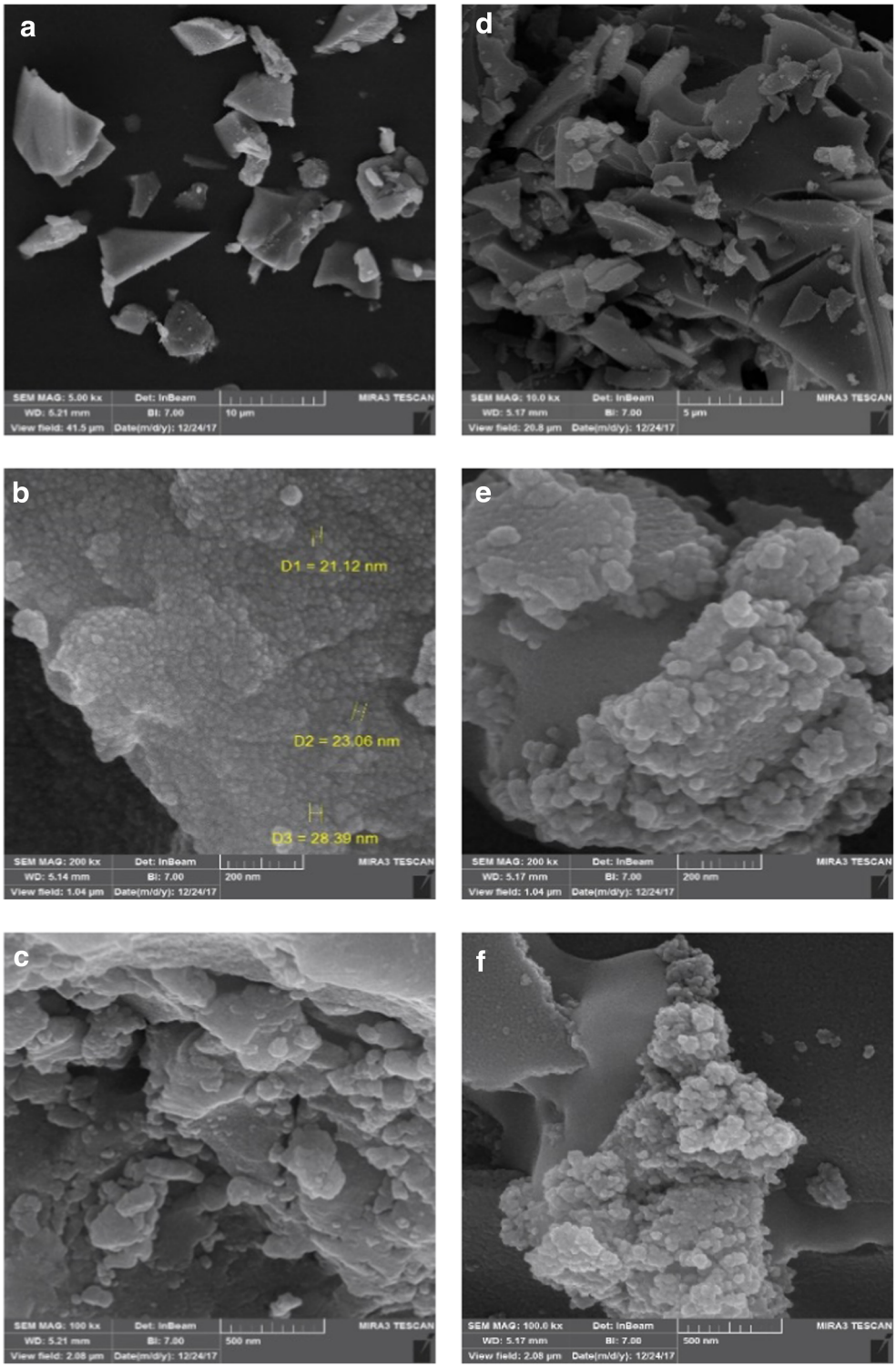

Fig. 3 FE-SEM images of synthesized nano- TiO_2 (**a**–**c**), and coated quartz tubes (**d**–**f**)

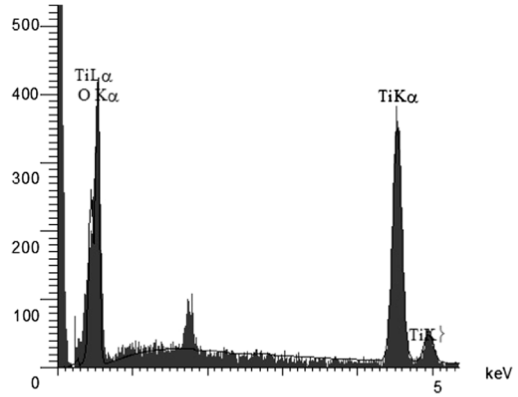

Quantitative Results

Elt	Line	Int	Error	K	Kr	W%	A%
O	Ka	93.8	25.6087	0.3770	0.1703	67.00	85.88
Ti	Ka	173.3	0.7897	0.6230	0.2814	33.00	14.12
				1.0000	0.4517	100.00	100.00

Fig. 4 EDX analysis of synthesized catalyst on quartz tubes

primary particle, which is a single crystal particle. The particle tested by SEM though, usually is a particle consisted of one or two, even more primary particles [36]. Crystal size could only calculated by Scherer equation and the size given by this equation is completely reliable. And the size given by SEM is particle size not crystal size [36].

EDX analysis in Fig. 4 confirms a good dispersion of TiO_2 nanoparticles on quartz tubes. As it can be seen, the catalyst was composed of Ti and O with a molar ratio close to 1:2 which confirms that the molecular formula of catalyst is TiO_2.

Effect of solution pH

To determine the optimum pH for maximum BP-3 removal, the effect of solution pH was studied and the obtained data were shown in Fig. 5. As it is shown in Fig. 5, the increase in pH value from 3 to 10 increased the BP-3 removal efficiency from 17 to 82%. In photocatalytic degradation, the removal efficiency is highly affected by catalyst's surface charge and substrate's ionic form. According to Eq. (5) in acidic solution with presence of H^+ ions, the surface of catalyst is charged positively. However, in alkaline solution, the surface of catalyst is charged negatively because of OH^- ions (Eq. 6).

$$Acidic\ solution\ TiOH + H^+ \leftrightarrow TiOH_2^+ \quad (5)$$

$$Alkaline\ solution\ TiOH + OH^- \leftrightarrow TiO^- + H_2O \quad (6)$$

In addition, the pKa of BP-3 is 8.06 [23] and under that BP-3 is found in its molecular form. It is also reported that benzophenone-derivatives are stabilized under acidic conditions [37] .In contrast, BP-3's phenolic group is deprotonated in more than this value and becomes more negative. As a result, an electronic repulsion between the substrate and the surface of catalyst, which is negatively charged in alkaline solution, increases. This repulsion prevents BP-3 to be adsorbed on the catalyst's surface. Though of course, pKa value is principal valid only in bulk solutions. In addition, the dissociation of the BP-3 could be related to form a double layer at the liquid- solid interface [20].

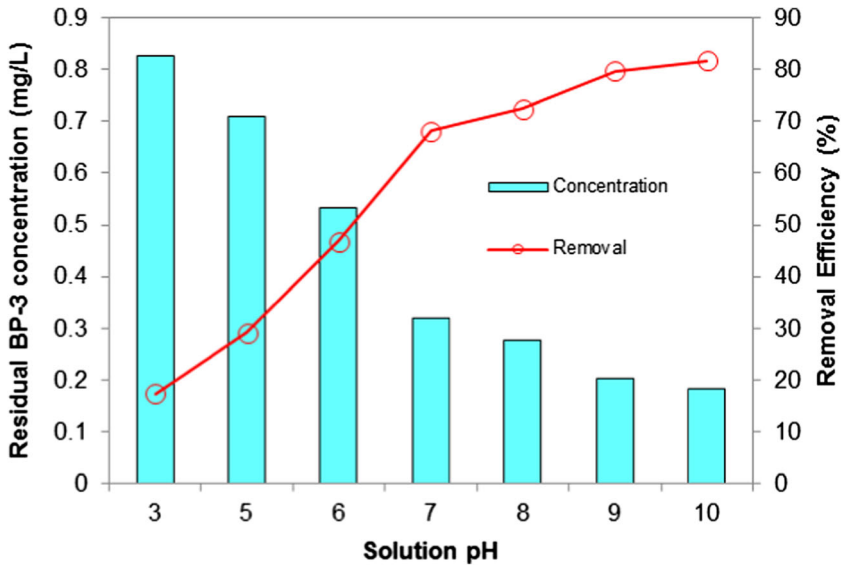

Fig. 5 Effect of initial solution pH on BP-3 degradation (Initial BP-3 concentration: 1 mg/L, catalyst surface area: 135 cm^2 and 15 min contact time)

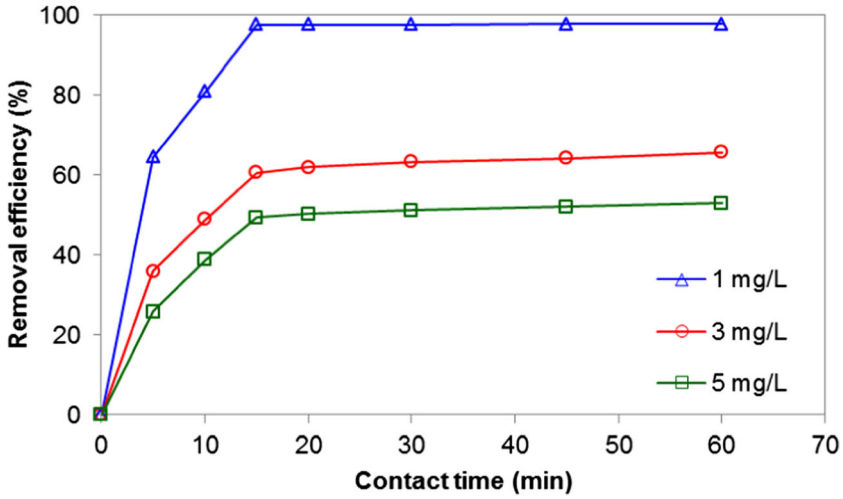

Fig. 6 Effect of contact time on BP-3 degradation (solution pH: 10 and catalyst surface area: 225 cm^2)

Furthermore, in higher pH more hydroxyl inions are generated. It improves hydroxyl radical generation. These radicals are responsible for BP-3 oxidation, so the more hydroxyl radicals are produced, the more removal efficiency occurs. It is also in agreement with a study which noticed that in alkaline solutions, hydroxyl ions on the surface of TiO_2 easily change to hydroxyl radicals. Thus, degradation efficiency of benzyl paraben improves [38].

Effect of contact time

The effect of contact time on BP-3 degradation was evaluated and the obtained data were shown in Fig. 6. As depicted in Fig. 6, with increasing the contact time from 5 to 15 min, degradation efficiency increased from 64 to 98%, 36 to 60% and 25 to 50% for 1, 3 and 5 mg/L of BP-3, respectively. It was observed that after 15 min, the degradation efficiency rate was constant (approximately 98%). Although a slight change (1%) in removal efficiency occurred after 15 min, it could be ignored.

In fact, during the reaction time more hydroxyl radicals are produced from hydroxyl ions that lead to more degradation of the pollutant [39]. Gago-Ferrero et al. (2013) studied BP-3 degradation with ozone and peroxone and showed that during 40–50 min, 95% degradation efficiency was observed [23]. The high degradation efficiency (around 98%) during 15 min in the present study proved the ability of synthesized catalyst for BP-3 degradation.

Kinetic and synergy of BP-3 photocatalytic degradation

Generally, the Langmuir-Hinshelwood (LH) kinetic model is the most appropriate model to describe the heterogeneous photo-catalytic degradation [38, 40].

$$r = \frac{-dC}{dt} = k_{LH}\theta = k_{LH}\left(\frac{K_{LH}C_{eq}}{1 + K_{LH}C_{eq}}\right) \quad (7)$$

Where r is the initial reaction rate of BP-3, C_{eq} is the equilibrium BP-3 concentration, K_{LH} is the adsorption constant onto the catalyst surface, and k_{LH} is the intrinsic reaction rate constant. At low concentration (ppm and less than ppm) $K_{LH}C_{eq}$ can be neglected with respect to 1, and Eq. (7) can be simplified to a first- order kinetic equation (Eq. (8)) [38].

$$r = \frac{-dC}{dt} = k_{LH}K_{LH}C_{eq} \leftrightarrow \ln\frac{C_e}{C_0} = -k_{app}t \quad (8)$$

Where k_{app} is the first- order kinetic apparent rate constant and C_0 is close to C_{eq} [20].

Figure 7 shows the kinetic plot. The BP-3 degradation fit the first-order kinetic model well ($R^2 > 0.94$). The k_{app} value was 0.2 ($R^2 > 0.94$), 0.048 ($R^2 > 0.92$) and 0.035 min^{-1} ($R^2 > 0.92$) for 1, 3 and 5 mg/L of initial BP-3 concentration, respectively. The results are in agreement with a study which reported that photocatalytic degradation of benzyl paraben with TiO_2 follows the first-order kinetic model [38]. First -order and pseudo-firs- order kinetics models have been reported in several studies for organic pollutant degradation [9, 17, 23].

As it is shown in Fig. 8, a significant enhancement of BP-3 degradation was observed during the process of combining UV light and synthesized TiO_2 catalyst. Eq. (9) was applied to evaluate the synergistic effect [19].

$$Sy = \frac{K_{TiO_2/UV}}{K_{UV} + K_{TiO_2}} \quad (9)$$

where Sy is the synergistic effect, $K_{TiO2/UV}$ is the rate of combine process, K_{UV} and K_{TiO2} are the rates of the individual processes. The constant rate of combined process was greater than the sum of constant rates calculated under UV photooxidation and TiO_2 adsorption. It is observed that with TiO_2/UV degradation process, the synergy factor increased threefold. It can be noted that during photocatalytic degradation process,

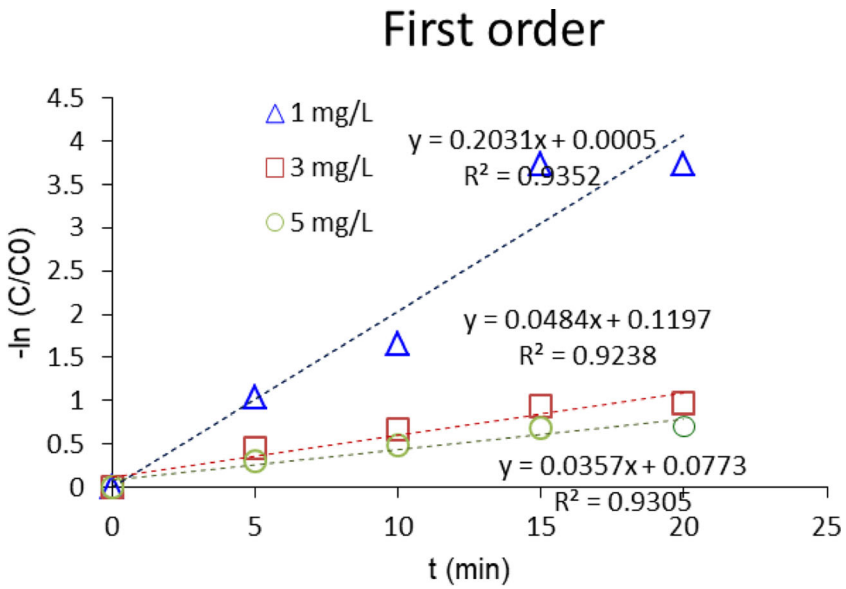

Fig. 7 Kinetic plot of BP-3 degradation (BP-3 concentration: 1 mg/L, solution pH: 10, catalysis surface area: 225 cm^2)

first, photo-excitation of TiO_2 leads to migration of electrons from balance band to the conduction band and holes (h^+) were left in the balance band. Then photo-generated electrons react with oxygen to produce superoxide anion radicals ($O_2^{-\bullet}$). Besides, reaction between holes and water results in hydroxyl radicals' generation. Hence, the degradation of BP-3 may promote via hydroxyl and superoxide radicals (Eq. (10–14)).

$$TiO_2 \xrightarrow{hv} h^+_{VB} + e^-_{CB} \quad (10)$$

$$H_2O + h^+_{VB} \rightarrow OH^\bullet + H^\bullet \quad (11)$$

$$O_2 + e^-_{CB} \rightarrow O_2^{-\bullet} \quad (12)$$

$$BP\text{–}3 + h^+_{VB} \rightarrow BP\text{–}3^+ \rightarrow Degradation\ products \quad (13)$$

$$BP\text{–}3 + O_2^{-\bullet}\ or\ OH^\bullet \rightarrow Degradation\ products \quad (14)$$

With the absence of UV light, photo-excitation of TiO_2 cannot be occurred and without excited electrons the radical generation is rare. On the other hand, with the absence of TiO_2 there is no excited electron, nor is there any hole to react with water. Therefore, the kinetic of each process individually is completely less than combined process. This result is also reported in the literature [19, 41, 42].

Effect of initial BP-3 concentration

Figure 9 illustrates the effect of initial BP-3 concentration on the degradation efficiency. Results demonstrated that with increasing the initial concentration of BP-3 from 1 to 5 mg/L, the degradation efficiency decreases from 98 to 47%. It can be explained by two reasons. The first one is because of catalyst-surface occupation by higher concentration of pollutant that leads to lack of active sites on the surface of the catalyst to

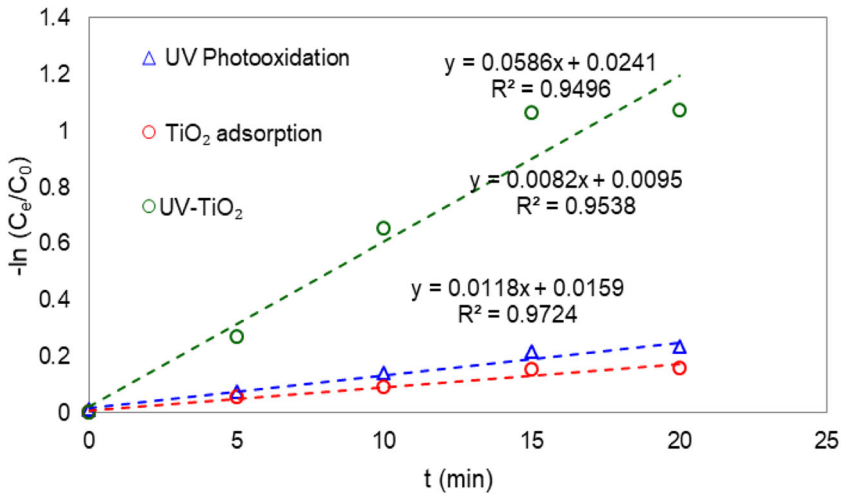

Fig. 8 Synergistic effect of combining UV photooxidation and TiO_2 adsorption on BP-3 photodegradation (BP-3 concentration: 1 mg/L, solution pH: 7, catalysis surface area: 135 cm^2)

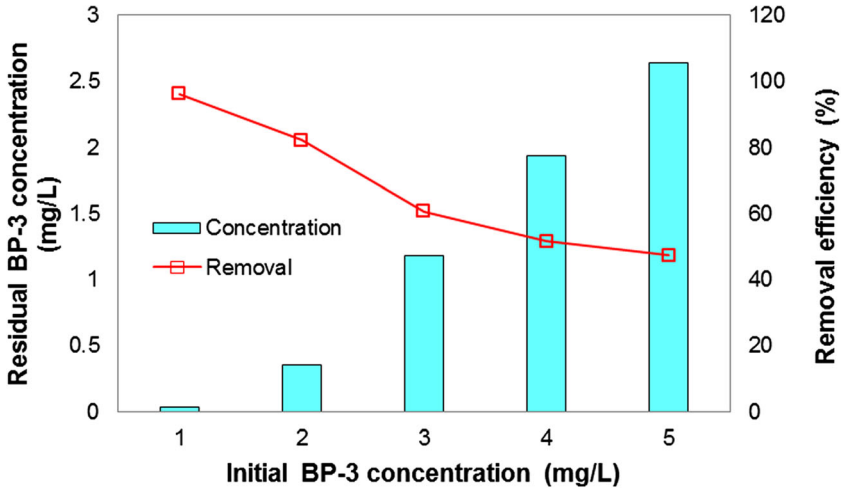

Fig. 9 Effect of initial concentration on BP-3 degradation (Solution pH: 10, catalyst surface area: 225 cm2 and contact time: 15 min)

enhance the degradation. The second one is that with increasing the concentration of the solution, UV photons can hardly penetrate into the solution and its path length becomes shorter. The lower absorption of photons prevents the photo-exciting of the surface of the catalyst and decreases the process of photodegradation. The same result has been reported in the photocatalytic degradation of other organic pollutant [39, 40, 43].

Effect of catalyst surface area

As it was shown in Fig. 10, when the surface area of catalyst increased from 45 to 225 cm^2, the degradation efficiency increased from 35.7 to 98%. It can be noted that with increasing the catalyst surface area, the TiO_2 amount on the coated tubes and also the number of active sites increased. In addition, with increasing TiO_2, more UV photons can be absorbed by the surface of the catalyst and more hydroxyl radicals and other reactive species can be produced that enhance the degradation process. It is in agreement with photocatalytic degradation studies of different organic compounds [20, 38]. The method used in this study, however, was superior to the other related studies because in those papers it was noted that with increasing the amount of TiO_2 more than a particular concentration, the catalyst particles were aggregated that resulted in reduction in light penetration which caused eventually a reduction in degradation [20, 38, 44, 45]. In contrast, in present study nanoparticles were coated on quartz tubes, so that no particles aggregation occurred.

Modeling of BP-3 degradation by RSM

In order to optimize the process of BP-3 degradation, it is necessary to evaluate the interaction between effective parameters. As it was mentioned before, the effect of 4 parameters including initial concentration of BP-3, the surface area of the catalyst, pH and reaction time was individually investigated and then selected as factors in CCD model

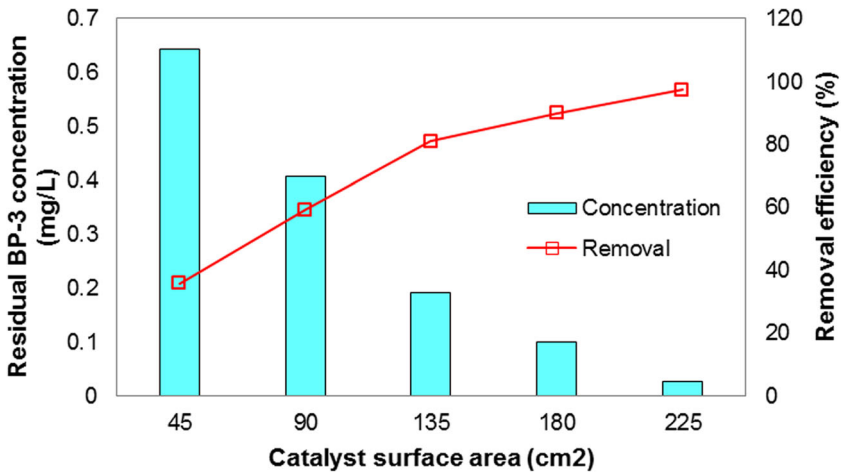

Fig. 10 Effect of catalyst surface area on BP-3 degradation (initial BP-3 concentration: 1 mg/L, solution pH: 10, and contact time: 15 min)

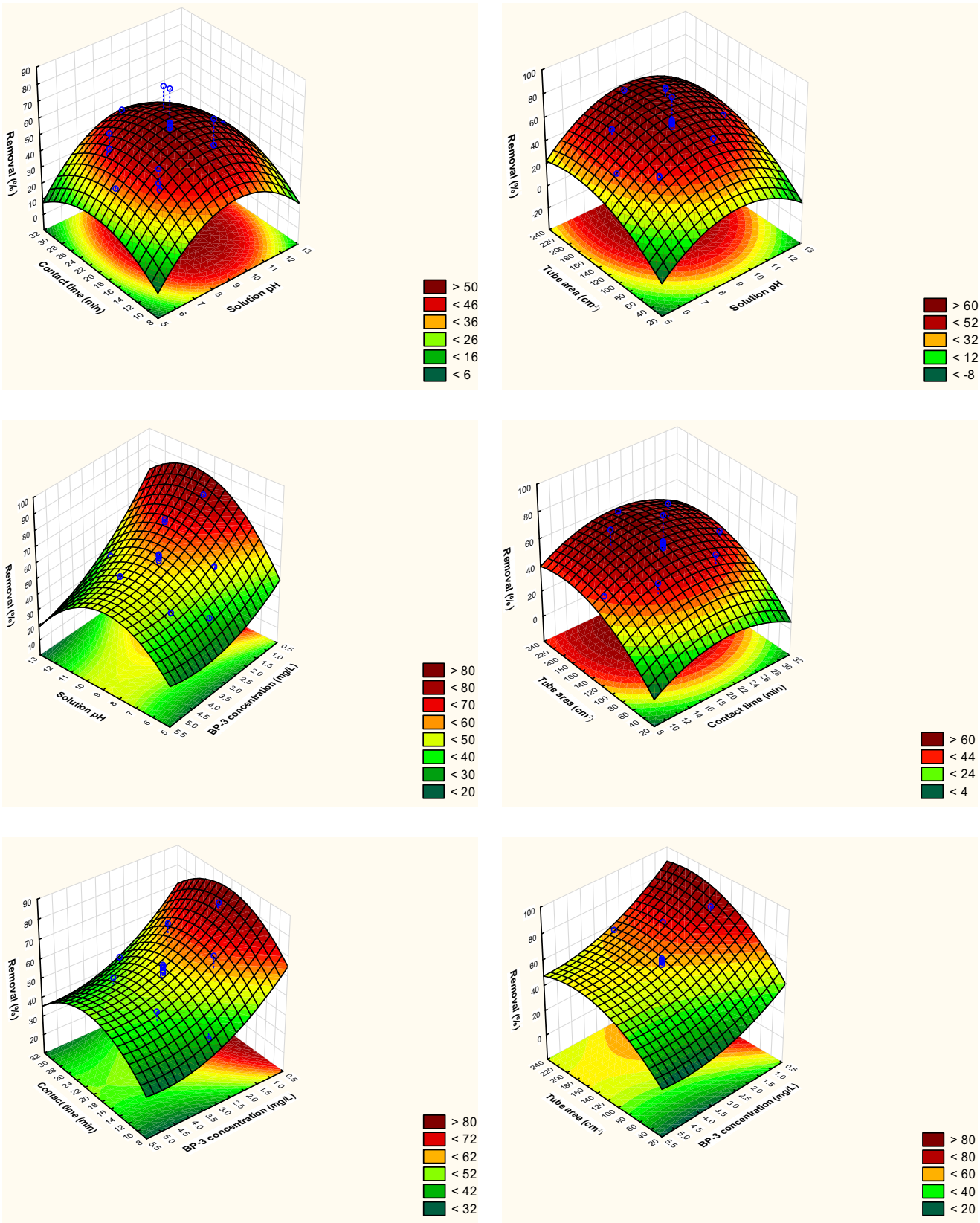

Fig. 11 Simultaneous effect of variables on degradation efficiency

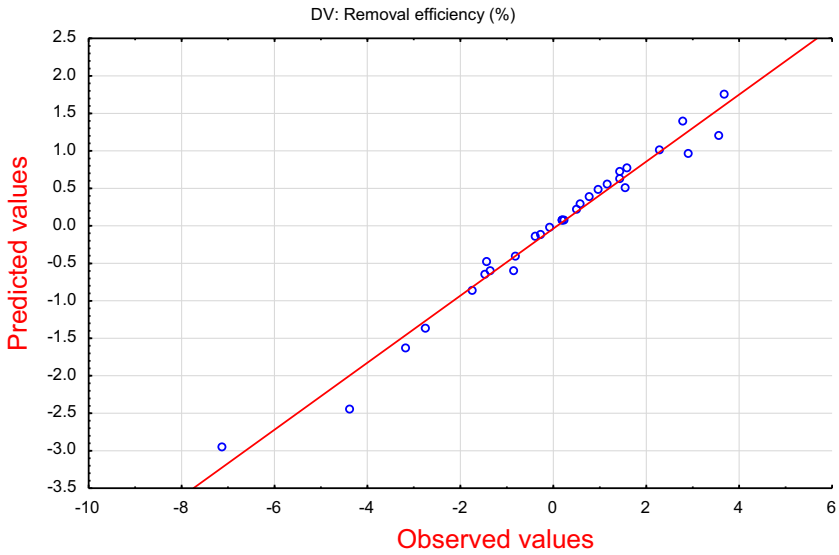

Fig. 12 The observed value plotted against predicted value of BP-3 photo-degradation

(Table 4). BP-3 degradation was modeled by the polynomial equation (Eq. 15).

$$R(\%) = 56.21 + 4.97p - 3.91p^2 + 0.89t - 2.91t^2 - 6.56c + 1.66c^2 + 6.97a - 2.87a^2 + 0.21pt - 1.5pc + 0.36pa - 0.07tc - 0.04ta - 0.64ca \quad (15)$$

where, p is the solution initial pH, t is reaction time (min), a is catalyst surface area (cm^2) and c is initial concentration of BP-3 (mg/L).

After removing non-significant terms including linear form of t (p-value: 0.2), interactions of pt (p-value: 0.79), pc (p-value: 0.07), pa (p-value: 0.65), tc (p-value: 0.92), ta (p-value: 0.95), ca (p-value: 0.44) from the initial model, final significant terms were modeled by Eq. (16).

$$R(\%) = 56.21 + 4.97p - 3.91p^2 - 2.91t^2 - 6.73c + 1.66c^2 + 7.01a - 2.87a^2 \quad (16)$$

Table 5 shows the comparison between predicted and experimental amount of BP-3 degradation percent. The value of the determination coefficient, R^2, was 96%, indicating a good conformity between experimental and predicted results.

Figure 11 shows the simultaneous effects of parameters on BP-3 photo-degradation. As it was mentioned before, increasing in pH value and the surface area of the catalyst promoted degradation efficiency due to higher amount of oxidative species and activated holes in which the oxidation- reduction processes improved. In contrast, as it was explained, the lower initial concentration resulted in an enhancement in the degradation efficiency. Figure 12 and Table 5 showed that RSM model was able to predict the degradation efficiency.

In order to evaluate the significance and adequacy of the regression model, analysis of variance (ANOVA) was applied. The results given in Table 8 establish that the model is high significant with probability value of 0.0001 and F value of 50.66. R^2 of the model was 0.9955 that means the model can

Table 8 ANOVA analysis for the response surface model

	Sum of squares	*df*	Mean square	F value	probability (*p*)
Regression model	3744.97	7	532	50.66	0.0001
p (L)	598.46	1	598.46	56.67	0.000002
p (Q)	449.90	1	449.90	42.60	0.00001
t (Q)	232.02	1	232.02	21.97	0.000292
a (L)	1147.55	1	1147.55	108.67	0.00000
a (Q)	225.49	1	225.49	21.35	0.00033
c (L)	1016.08	1	1016.08	96.22	0.00000
c (Q)	75.47	1	75.47	7.14	< 0.0001
Residual	173.1	22	7.8		
Lack of fit	14.71	7	2.1	0.89	0.76
Error	158.39	15	10.56		
Total	3918.07	29			

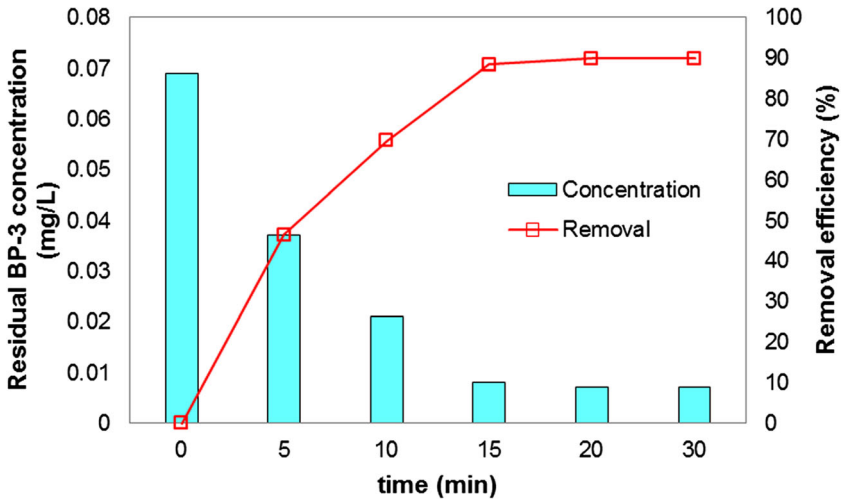

Fig. 13 BP-3 photo-degradation in the swimming pool water (Solution pH: 7.5, catalyst surface: 225 cm^2)

explain 99.55% of variables for BP-3 degradation and only 0.45% of variables cannot be explained by the model. In addition, adjusted R^2 (Adj-R^2) 0.982 showed a proper adjustment of the regression model to the observed results. The amount of lack of fit can also demonstrate the validation of the model. The p value of lack of fit was 0.76 which showed that the lack of fit was not significant. The correlation between experimental and predicted results in Fig. 12 confirms that the model has a satisfactory approximation to the observed results.

BP-3 photocatalytic degradation in swimming pool

In order to prove the ability of photocatalytic process for the real aqueous solutions, BP-3 degradation in swimming pool water was examined. The properties of swimming pool were shown in Table 2. The experiments were repeated for three times and the obtained results were shown in Fig. 13. As seen in Fig. 13, the application of the photocatalytic process led to 88% BP-3 degradation efficiency. Based on the obtained results, the photocatalytic process could successfully be applied to treat swimming pools water with low turbidity.

BP-3 photocatalytic degradation in wastewater treatment plant

In order to investigate the ability of the photocatalytic method for BP-3 degradation in wastewater treatment plant, the collected wastewater was examined. The properties of wastewater were shown in Table 3. The experiments were repeated for three times and the obtained results were shown in Fig. 14. As seen in Fig. 14, the application of the photocatalytic process led to 32.1% BP-3 degradation efficiency after 60 min. Based on the obtained results, the photocatalytic process could hardly be applied for BP-3 degradation in raw wastewater. The high turbidity causes the reduction in removal efficiency. The same result was reported by Li et al. (2007) who studied occurrence and behavior of four of the most used sunscreen

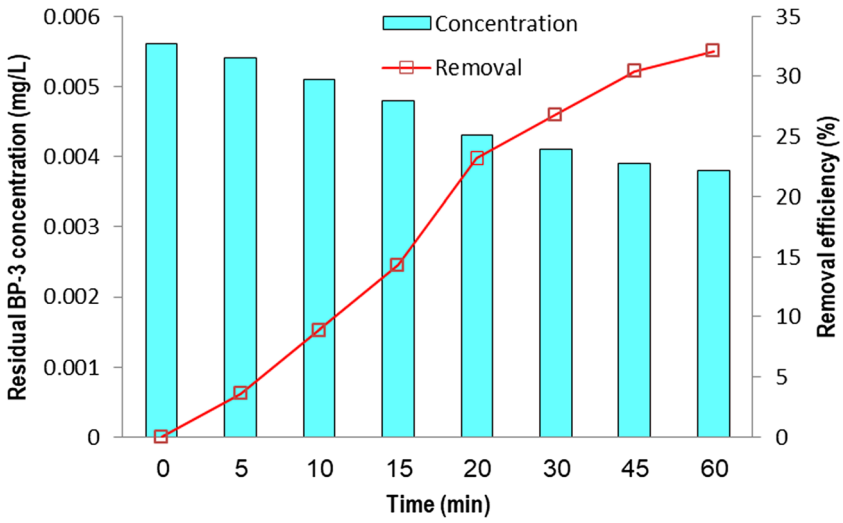

Fig. 14 BP-3 photo-degradation in wastewater treatment plant (Solution pH: 7.5, catalyst surface: 225 cm^2)

UV filters in a wastewater treatment plant and achieved only 20% BP-3 removal after 180 min using AOP [46]. Rosal et al. (2010) also found that using biological and AOP method for BP-3 removal in wastewater treatment plant resulted in no BP-3 removal after 15 min [47].

Conclusion

The results of this study showed that TiO_2 nanoparticles coated on quartz is an efficient catalyst for BP-3 degradation in aqueous solution with low turbidity. The photocatalytic degradation, however, would be hampered in aqueous solution with high turbidity like raw wastewater.

In this study under optimum condition (initial BP-3 concentration 1 mg/L, pH 10, the catalyst surface area 225 cm^2) after 15 min 98% of BP- 3 was removed form synthetic wastewater. BP-3 removal process was fitted to the first-order kinetic model. 88% of BP-3 initial concentration was also removed after 25 min from swimming pool water.

The advantage of this study was that during the photocatalytic degradation using coated quartz no agglomeration of nanoparticles occurred. Also based on the obtained results, and according to the fact that the applied method is easy to operate and economic and the catalyst could be applied repeatedly, the method is suggested for BP-3 removal in swimming pools. The other advantage of this study is that using TiO_2 coated on quartz would reduce the health risk of existence of TiO_2 in the effluent. But this issue can be studied in full scale in the next studies.

The limitation and disadvantage of this method is that in aqueous solutions with high turbidity the photocatalytic process would be hampered due to agglomeration of particles in solution. This study showed that the method could hardly remove BP-3 from wastewater in 60 min with only 32.1% removal efficiency.

For the next studies we suggest AOP method including photocatalytic method to be used for BP-3 removal in secondary and tertiary refined effluent. Also according to the results of this study we suggest to investigate the existence of BP-3 in swimming pools which necessitate shower before entering to the pool.

According to our results we suggest using the photocatalytic process with TiO_2 coated on quartz tubes for water treatment in swimming pools.

Acknowledgements This research was financially supported by Isfahan University of Medical Sciences under #396490 and ethics code: IR.MUI.REC.1396.3.490.

Compliance with ethical standards

Conflict of interest The authors declare that they have no conflict of interest.

References

1. Gago-Ferrero P, Badia-Fabregat M, Olivares A, Pina B, Blanquez P, Vicent T, et al. Evaluation of fungal- and photo-degradation as potential treatments for the removal of sunscreens BP3 and BP1. Sci Total Environ. 2012;427:355–63.
2. Cunha SC, Trabalon L, Jacobs S, Castro M, Fernandez-Tejedor M, Granby K, et al. UV-filters and musk fragrances in seafood commercialized in Europe union: occurrence, risk and exposure assessment. Environ Res. 2018;161:399–408.
3. Schlumpf M, Kypke K, Wittassek M, Angerer J, Mascher H, Mascher D, et al. Exposure patterns of UV filters, fragrances, parabens, phthalates, organochlor pesticides, PBDEs, and PCBs in human milk correlation of UV filters with use of cosmetics. Chemosphere. 2010;81(10):1171–83.
4. Kim S, Choi K. Occurrences, toxicities, and ecological risks of benzophenone-3, a common component of organic sunscreen products: a mini-review. Environ Int. 2014;70:143–57.
5. Molins-Delgado D, Olmo-Campos MD, Valeta-Juan G, Pleguezuelos-Hernandez V, Barcelo D, Diaz-Cruz MS. Determination of UV filters in human breast milk using turbulent flow chromatography and babies' daily intake estimation. Environ Res. 2018;161:532–9.
6. Garcia HA, Hoffman CM, Kinney KA, Lawler DF. Laccase-catalyzed oxidation of oxybenzone in municipal wastewater primary effluent. Water Res. 2011;45(5):1921–32.
7. Cochrane AM, Cheung C, Rangan K, Freyer D, Nahata L, Dhall G, et al. Long-term follow-up of endocrine function among young children with newly diagnosed malignant central nervous system tumors treated with irradiation-avoiding regimens. Pediatr Blood Cancer. 2017;64(11)
8. Kunisue T, Chen Z, Louis GMB, Sundaram R, Hediger ML, Sun LP, et al. Urinary concentrations of Benzophenone-type UV filters in U.S. women and their association with endometriosis. Environ Sci Technol. 2012;46(8):4624–32.
9. Yang B, Ying GG. Oxidation of benzophenone-3 during water treatment with ferrate(VI). Water Res. 2013;47(7):2458–66.
10. Gonzalez H, Farbrot A, Larko O, Wennberg AM. Percutaneous absorption of the sunscreen benzophenone-3 after repeated whole-body applications, with and without ultraviolet irradiation. Br J Dermatol. 2006;154(2):337–40.
11. Balmer ME, Buser HR, Muller MD, Poiger T. Occurrence of some organic UV filters in wastewater, in surface waters, and in fish from Swiss lakes. Environ Sci Technol. 2005;39(4):953–62.
12. Molins-Delgado D, Manez M, Andreu A, Hiraldo F, Eljarrat E, Barcelo D, et al. A potential new threat to wild life: presence of UV filters in bird eggs from a preserved area. Environ Sci Technol. 2017;51(19):10983–90.
13. Campos D, Gravato C, Fedorova G, Burkina V, Soares A, Pestana JLT. Ecotoxicity of two organic UV-filters to the freshwater caddisfly Sericostoma vittatum. Environ Pollut. 2017;228:370–7.
14. Rodil R, Quintana JB, Concha-Grana E, Lopez-Mahia P, Muniategui-Lorenzo S, Prada-Rodriguez D. Emerging pollutants in sewage, surface and drinking water in Galicia (NW Spain). Chemosphere. 2012;86(10):1040–9.
15. Kameda Y, Kimura K, Miyazaki M. Occurrence and profiles of organic sun-blocking agents in surface waters and sediments in Japanese rivers and lakes. Environ Pollut. 2011;159(6):1570–6.
16. Krzeminski P, Schwermer C, Wennberg A, Langford K, Vogelsang C. Occurrence of UV filters, fragrances and organophosphate flame retardants in municipal WWTP effluents and their removal during membrane post-treatment. J Hazard Mater. 2017;323:166–76.
17. Natarajan K, Natarajan TS, Bajaj HC, Tayade RJ. Photocatalytic reactor based on UV-LED/TiO2 coated quartz tube for degradation of dyes. Chem Eng J. 2011;178:40–9.

18. Tzikalos N, Belessi V, Lambropoulou D. Photocatalytic degradation of reactive red 195 using anatase/brookite TiO2 mesoporous nanoparticles: optimization using response surface methodology (RSM) and kinetics studies. Environ Sci Pollut Res. 2013;20(4): 2305–20.
19. Na S, Ahn YG, Cui M, Khim J. Significant diethyl phthalate (DEP) degradation by combined advanced oxidation process in aqueous solution. J Environ Manag. 2012;101:104–10.
20. Zuniga-Benitez H, Aristizabal-Ciro C, Penuela GA. Heterogeneous photocatalytic degradation of the endocrine-disrupting chemical Benzophenone-3: parameters optimization and by-products identification. J Environ Manag. 2016;167:246–58.
21. Misra NN. The contribution of non-thermal and advanced oxidation technologies towards dissipation of pesticide residues. Trends Food Sci Technol. 2015;45(2):229–44.
22. Brillas E, Mur E, Sauleda R, Sànchez L, Peral J, Domènech X, et al. Aniline mineralization by AOP's: anodic oxidation, photocatalysis, electro-Fenton and photoelectro-Fenton processes. Appl Catal B Environ. 1998;16(1):31–42.
23. Gago-Ferrero P, Demeestere K, Diaz-Cruz MS, Barcelo D. Ozonation and peroxone oxidation of benzophenone-3 in water: effect of operational parameters and identification of intermediate products. Sci Total Environ. 2013;443:209–17.
24. Gong P, Yuan H, Zhai P, Xue Y, Li H, Dong W, et al. Investigation on the degradation of benzophenone-3 by UV/H2O2 in aqueous solution. Chem Eng J. 2015;277:97–103.
25. Pan X, Yan L, Li C, Qu R, Wang Z. Degradation of UV-filter benzophenone-3 in aqueous solution using persulfate catalyzed by cobalt ferrite. Chem Eng J. 2017;326:1197–209.
26. Hu H, Xiao WJ, Yuan J, Shi JW, Chen MX, Shang GWF. Preparations of TiO2 film coated on foam nickel substrate by sol-gel processes and its photocatalytic activity for degradation of acetaldehyde. J Environ Sci. 2007;19(1):80–5.
27. Amini M, Younesi H, Bahramifar N, Lorestani AAZ, Ghorbani F, Daneshi A, et al. Application of response surface methodology for optimization of lead biosorption in an aqueous solution by Aspergillus Niger. J Hazard Mater. 2008;154(1–3):694–702.
28. Aquino JM, Rocha-Filho RC, Bocchi N, Biaggio SR: Electrochemical degradation of the Disperse Orange 29 dye on a β-PbO2 anode assessed by the response surface methodology. J Environ Chem Eng. 2013;1(4):954–961.
29. Ghasemi Z, Younesi H, Zinatizadeh AA. Preparation, characterization and photocatalytic application of TiO2/Fe-ZSM-5 nanocomposite for the treatment of petroleum refinery wastewater: Optimization of process parameters by response surface methodology. Chemosphere. 2016;159:552–564.
30. Aksu Z, Gönen F. Binary biosorption of phenol and chromium(VI) onto immobilized activated sludge in a packed bed: Prediction of kinetic parameters and breakthrough curves. Sep Purif Technol. 2006;49(3):205–216.
31. Göksungur Y, Üren S, Güvenç U. Biosorption of cadmium and lead ions by ethanol treated waste baker's yeast biomass. Bioresour Technol. 2005;96(1):103–109.
32. Tarazona I, Chisvert A, Leon Z, Salvador A: Determination of hydroxylated benzophenone UV filters in sea water samples by dispersive liquid-liquid microextraction followed by gas chromatography-massspectrometry. J Chromatogr A. 2010;1217(29): 4771–4778.
33. Barroso M, Dias M, Vieira DN, Queiroz JA, Lopez-Rivadulla M. Development and validation of an analytical method for the simultaneous determination of cocaine and its main metabolite, benzoylecgonine, in human hair by gas chromatography/mass spectrometry. Rapid Commun. Mass Spectrom. 2008;22(20):3320–3326.
34. Liu Y-S, Ying G-G, Shareef A, Kookana RS. Occurrence and removal of benzotriazoles and ultraviolet filters in a municipal wastewater treatment plant. Environ Pollut. 2012;165:225–232.
35. Domingos R, Baalousha M, Ju-Nam Y, Reid M, Tufenkji N, R Lead J, Leppard G, Wilkinson K. Characterizing Manufactured Nanoparticles in the Environment: Multimethod Determination of Particle Sizes. Environ Sci Technol. 2009;43(19):7277–7284.
36. Hargreaves JSJ. Some considerations related to the use of the Scherrer equation in powder X-ray diffraction as applied to heterogeneous catalysts. Catal Struct React. 2016;2(1-4):33–37.
37. Bluthgen N, Zucchi S, Fent K. Effects of the UV filter benzophenone-3 (oxybenzone) at low concentrations in zebrafish (Danio rerio). Toxicol Appl Pharmacol. 2012;263(2):184–194.
38. Lin Y, Ferronato C, Deng N, Chovelon J-M. Study of benzylparaben photocatalytic degradation by TiO2. Appl Catal B. 2011;104(3):353–360.
39. Zarean M, Bina B, Ebrahimi A. The influence of zero- Valent Iron on the Photodegradation ozonation of Di-2- Ethylhexyl phthalate in aqueous solution. Desalin Water Treat. 2017;78:321–9.
40. Zhao C, Pelaez M, Dionysiou DD, Pillai SC, Byrne JA, O'Shea KE. UV and visible light activated TiO2 photocatalysis of 6-hydroxymethyl uracil, a model compound for the potent cyanotoxin cylindrospermopsin. Catal Today. 2014;224:70–6.
41. Wu C, Liu X, Wei D, Fan J, Wang L. Photosonochemical degradation of phenol in water. Water Res. 2001;35(16):3927–33.
42. Malato S, Fernández-Ibáñez P, Maldonado MI, Blanco J, Gernjak W. Decontamination and disinfection of water by solar photocatalysis: recent overview and trends. Catal Today. 2009;147(1):1–59.
43. Chen CC, Lu CS, Chung YC, Jan JL. UV light induced photodegradation of malachite green on TiO2 nanoparticles. J Hazard Mater. 2007;141(3):520–8.
44. Affam AC, Chaudhuri M. Degradation of pesticides chlorpyrifos, cypermethrin and chlorothalonil in aqueous solution by TiO2 photocatalysis. J Environ Manag. 2013;130:160–5.
45. Lopez-Alvarez B, Torres-Palma RA, Penuela G. Solar photocatalitycal treatment of carbofuran at lab and pilot scale: effect of classical parameters, evaluation of the toxicity and analysis of organic by-products. J Hazard Mater. 2011;191(1–3):196–203.
46. Li W, Ma Y, Guo C, Hu W, Liu K, Wang Y, et al. Occurrence and behavior of four of the most used sunscreen UV filters in a wastewater reclamation plant. Water Res. 2007;41(15):3506–12.
47. Rosal R, Rodríguez A, Perdigón-Melón JA, Petre A, García-Calvo E, Gómez MJ, et al. Occurrence of emerging pollutants in urban wastewater and their removal through biological treatment followed by ozonation. Water Res. 2010;44(2):578–88.